THE JOURNAL OF NAVIGATION (2018), **71**, 1143–1160.
doi:10.1017/S0373463318000139

A Feasibility Study of Applying Laser Line Scanning to AUV Hydrodynamic Parameter Identification

Yu-Cheng Chou, Madoka Nakajima and Hsin-Hung Chen

(*Institute of Undersea Technology, National Sun Yat-sen University, 70 Lienhai Rd., Kaohsiung 80424, Taiwan*)
(E-mail: ycchou@mail.nsysu.edu.tw)

Precise control is a key factor in enabling Unmanned Underwater Vehicles (UUVs) to complete various underwater activities. The development of UUV control rules is mostly based on UUV dynamic models. However, such dynamic models contain unknown hydrodynamic parameters that need to be identified. This paper presents a new method, Laser Line Scanning for Hydrodynamic Parameter Identification (LSHPI), which integrates laser line scanning, decoupled dynamics, and evolutionary optimisation to identify the hydrodynamic parameters of an Autonomous Underwater Vehicle (AUV). In this research, laser images, seen from an on board camera's perspective and created using Open Graphics Library (OpenGL), were used to validate LSHPI's feasibility. The accuracy of the AUV positions and Euler angles obtained by the laser image-based methods were investigated for each decoupled One-Dimensional (1D) motion and the influence of other motion disturbances on the accuracy of the obtained AUV positions or Euler angles was also evaluated. In addition, the accuracy of the surge-related hydrodynamic parameters obtained by LSHPI was investigated under different motion disturbances. Based on the hydrodynamic parameter identification results under different motion disturbances, LSHPI's feasibility was successfully validated.

KEYWORDS

1. Autonomous underwater vehicle. 2. Hydrodynamic parameter identification. 3. Laser line scanning. 4. Genetic algorithm.

Submitted: 2 October 2017. Accepted: 23 February 2018. First published online: 30 April 2018.

1. INTRODUCTION. Unmanned Underwater Vehicles (UUVs), including Autonomous Underwater Vehicles (AUVs) and Remotely Operated Vehicles (ROVs), are used to perform various tasks in ocean and seabed exploration and investigation. One of the key enabling factors in UUV operations, especially near the seabed, is the precise control of the UUV itself. The development of UUV control rules is mostly based on UUV dynamic models. However, such dynamic models essentially contain a number of unknown hydrodynamic parameters. Thus, in order to achieve precise control of UUVs, it is important

to have an effective and accurate system identification method. System identification for a UUV requires estimation of the UUV's hydrodynamic parameters using experimental data. Planar Motion Mechanisms (PMMs), on board sensors and vision technologies are three main approaches to acquire data from UUV motion experiments.

The PMM-based identification method requires that motion experiments have to be conducted using an original or scaled UUV in a large water tank (Avila et al., 2012; Nakamura et al., 2013; Nomoto and Hattori, 1986). With the measured forces and torques exerted on a UUV, the UUV's hydrodynamic parameters can be calculated through signal processing techniques. Even though the PMM-based method is the most straightforward approach for UUV system identification, it is expensive, and its accuracy is significantly affected by the scaling of the UUV.

Depending on the functions of the sensors, the on board sensor-based method can obtain a UUV's position data (Caccia et al., 2000; Smallwood and Whitcomb, 2003) or velocity and acceleration data (Avila et al., 2013; Farrell and Clauberg, 1993; Martin and Whitcomb, 2014; Valeriano-Medina et al., 2013). Through measured data and different algorithms, such as the Kalman filter and Least Squares (LS) method, the UUV's hydrodynamic parameters can be identified. The on board sensor-based method is highly cost-effective and repeatable, and is particularly suitable for UUVs whose payload and configuration must change to satisfy the requirements of different tasks (Caccia and Veruggio, 2000).

The vision technology-based method can obtain accurate position data for a UUV, and due to its low cost feature, it is an appealing approach to building the navigation system of a UUV (Gracias et al., 2003; Negahdaripour and Xu, 2002). More importantly, either through an on board camera (Ridao et al., 2004) or a camera outside a water tank (Chen, 2008), this method achieves accuracy and low cost.

This paper presents a new method, Laser Line Scanning for Hydrodynamic Parameter Identification (LSHPI), which integrates laser line scanning, decoupled dynamics, and evolutionary optimisation to identify the hydrodynamic parameters of an AUV/UUV. The concept of the laser line scanning technique of LSHPI is based on the method proposed in Wang and Cheng (2007). To extract information from photographs, a widely used approach is the stereovision technique, which is classified as a passive vision technique and works well unless the photographs have only smoothly textured areas, repetitive structures, or unclear images. To overcome this limitation and increase the image Signal-to-Noise Ratio (SNR), we adopt an active vision technique, which projects structured light onto the scene and infers detailed information of various features from the distortion of the structured light in the image. A light stripe generated by a laser source is a commonly adopted structured light pattern. For acquiring real-world position information from images, which directly relates to camera calibration for underwater experiments, LSHPI adopts the method proposed in Wang and Cheng (2007). The method uses only a board to implement the calibration scheme, which is easier than other approaches that require a rigid control frame. In addition, LSHPI also has the following advantages: it has a high sampling rate, it is cost-effective, it has high spatial resolution and once the camera calibration has been done, it does not require re-calibration. Finally, it does not require the accurate dimensions of the experimental area.

2. LASER LINE SCANNING FOR HYDRODYNAMIC PARAMETER IDENTIFICATION.

The proposed method, Laser Line Scanning for Hydrodynamic Parameter

https://doi.org/10.1017/S0373463318000139 Published online by Cambridge University Press

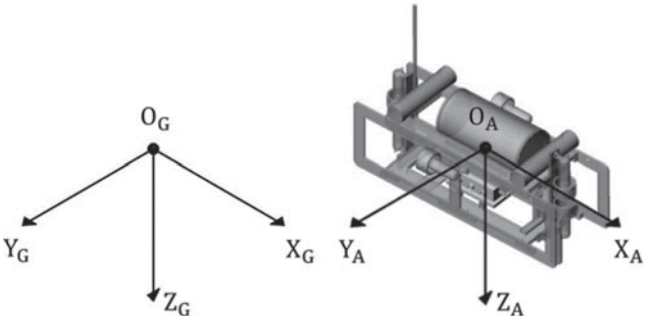

Figure 1. Earth-fixed and body-fixed coordinate systems.

Identification (LSHPI), integrates laser line scanning, decoupled dynamics, and evolutionary optimisation to identify AUV hydrodynamic parameters. The LSHPI contains three main steps: firstly, conduct AUV 1D motion experiments; secondly, obtain AUV positions or Euler angles through laser images and finally, obtain AUV hydrodynamic parameters through evolutionary optimisation.

An AUV equipped with a laser imaging system is commanded to perform six decoupled 1D motions to acquire a series of laser images. Each 1D motion corresponds to a translational or a rotational Degree Of Freedom (DOF). Among the six 1D motions, surge, sway and yaw motions require a specific object to be placed at the bottom of a water tank for laser scanning purposes, whereas heave, roll and pitch motions do not require an object.

Before obtaining the AUV positions or Euler angles, an important task is to locate the laser line positions on the laser scanning plane through laser images. With the obtained laser line positions and necessary geometrical parameters of the target AUV, the AUV positions or Euler angles can be obtained through calculations.

Each 1D motion corresponds to a different set of hydrodynamic parameters. Thus, all of the AUV's hydrodynamic parameters can be obtained through identifying the hydrodynamic parameters relevant to each 1D motion, which is formulated as an optimisation problem in this research. In other words, for each 1D motion, the objective is to find a set of hydrodynamic parameters leading to a 1D equation of motion that minimises the differences between the experimental and predicted position/attitude data.

2.1. *Hydrodynamic parameters for decoupled motions.* To derive the equations of motion for an AUV, two coordinate systems, including the earth-fixed coordinate system $X_GY_GZ_G$ and the body-fixed coordinate system $X_AY_AZ_A$, are defined and shown in Figure 1.

With the assumptions adopted from Fossen (1994), the AUV equations of motion in the body-fixed coordinate system are obtained as follows:

$$\begin{cases} \dot{u} = [(Z_{\dot{w}} - m)wq + (m - Y_{\dot{v}})vr + (X_u + X_{u|u|}|u|)u + X]/(m - X_{\dot{u}}) \\ \dot{v} = [(X_{\dot{u}} - m)ur + (m - Z_{\dot{w}})wp + (Y_v + Y_{v|v|}|v|)v + Y]/(m - Y_{\dot{v}}) \\ \dot{w} = [(Y_{\dot{v}} - m)vp + (m - X_{\dot{u}})uq + (Z_w + Z_{w|w|}|w|)w + Z]/(m - Z_{\dot{w}}) \\ \dot{p} = [(Z_{\dot{w}} - Y_{\dot{v}})wv + (I_y - I_z + N_{\dot{r}} - M_{\dot{q}})rq + (K_p + K_{p|p|}|p|)p + r_{B_Z}mg\cos\theta\sin\phi + K]/(I_x - K_{\dot{p}}) \\ \dot{q} = [(X_{\dot{u}} - Z_{\dot{w}})uw + (I_z - I_x + K_{\dot{p}} - N_{\dot{r}})pr + (M_q + M_{q|q|}|q|)q + r_{B_Z}mg\sin\theta + M]/(I_y - M_{\dot{q}}) \\ \dot{r} = [(Y_{\dot{v}} - X_{\dot{u}})vu + (I_x - I_y + M_{\dot{q}} - K_{\dot{p}})pq + (N_r + N_{r|r|}|r|)r + N]/(I_z - N_{\dot{r}}) \end{cases} \quad (1)$$

https://doi.org/10.1017/S0373463318000139 Published online by Cambridge University Press

Table 1. Relations between hydrodynamic parameters and 1D motions.

1D motion	Hydrodynamic parameters	1D motion	Hydrodynamic parameters
Surge	$X_{\dot{u}}$, X_u, $X_{u\|u\|}$	Roll	$K_{\dot{p}}$, K_p, $K_{p\|p\|}$
Sway	$Y_{\dot{v}}$, Y_v, $Y_{v\|v\|}$	Pitch	$M_{\dot{q}}$, M_q, $M_{q\|q\|}$
Heave	$Z_{\dot{w}}$, Z_w, $Z_{w\|w\|}$	Yaw	$N_{\dot{r}}$, N_r, $N_{r\|r\|}$

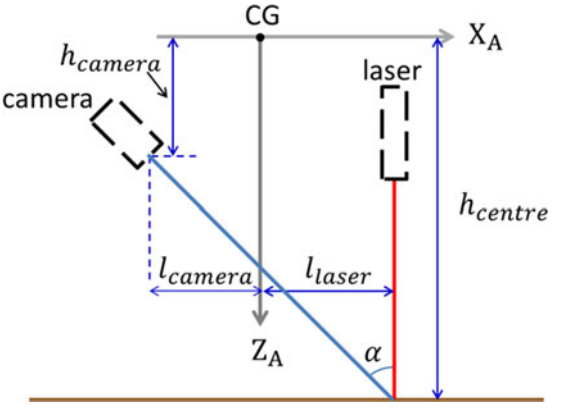

Figure 2. Assumed geometrical relations among the CG, video camera, and laser module of the AUV.

where X, Y and Z are forces; K, M and N are torques; u, v and w are translational velocities with respect to $X_AY_AZ_A$; p, q and r are angular velocities with respect to $X_AY_AZ_A$; x, y and z are positions with respect to $X_GY_GZ_G$ and ϕ, θ and ψ are Euler angles with respect to $X_GY_GZ_G$. m is the mass and I_x, I_y and I_z are the moments of inertia about $X_AY_AZ_A$. r_{B_Z} is the vertical component of the position vector from the Centre of Gravity (CG) to the Centre of Buoyancy (CB). g is the gravitational acceleration and the remaining 18 parameters ($X_{\dot{u}}$, X_u, $X_{u|u|}$, etc.) are the hydrodynamic parameters to be identified through six 1D motions. Table 1 shows the relations between hydrodynamic parameters and decoupled 1D motions.

2.2. *Laser image-based AUV position and attitude calculations.* The uniqueness of LSHPI is in determining the AUV positions and Euler angles through laser images. The procedures to calculate the AUV positions or Euler angles in each decoupled motion will be presented in the following subsections. Figure 2 shows the assumed geometrical relations between the CG, video camera and laser module of the AUV. All four lengths, including h_{camera}, h_{centre}, l_{camera} and l_{laser} can be acquired beforehand and are considered as given information.

2.2.1. *Surge motion.* The scanned object for the surge motion has two layers: the upper layer consists of multiple hexagon components; which have the same dimensions and connect one after another. The lower layer is a rectangular board, which is used to locate the scanned object's centre line in a laser image. In general, an AUV cannot initiate a path parallel to the scanned object's centre line, as shown in Figure 3. Thus, before calculating the AUV positions, the angle ψ_S between the AUV moving path and the scanned object's centre line has to be determined through laser images.

https://doi.org/10.1017/S0373463318000139 Published online by Cambridge University Press

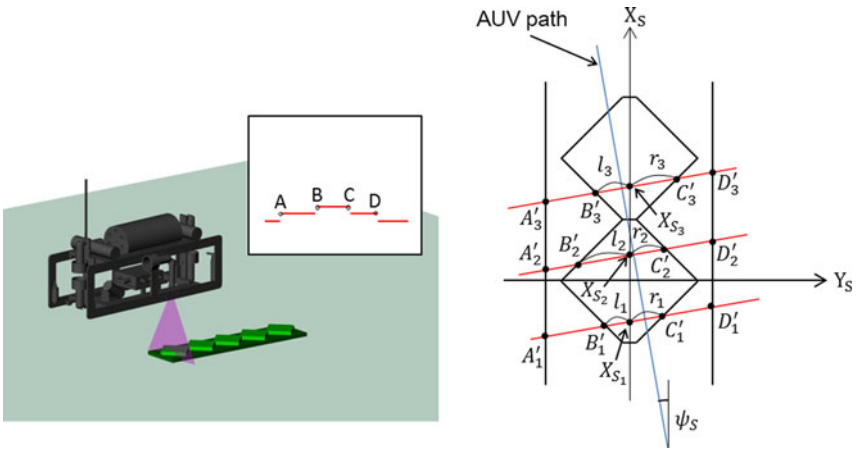

Figure 3. Laser image-based AUV position calculation for surge motion.

The procedure to calculate the AUV positions in surge motion is as follows:

1. Obtain the angle ψ_S between the AUV moving path and the scanned object's centre line.
   (a) For points A, B, C and D on each of the n laser images, convert their horizontal pixel coordinates to the horizontal coordinates on the laser scanning plane.
   (b) Calculate the lengths l_i and r_i, which are the distances from the scanned object's centre line to points B'_i and C'_i, respectively. The scanned object's centre line is located at the centres between points A'_i and D'_i, where $i = 1, 2, \cdots, n$.
   (c) Calculate the angles ψ_{S_i} using l_i and r_i, where $i = 1, 2, \cdots, n$. Then find the mean angle ψ_S.
2. Obtain the AUV positions x_i along the moving path.
   (a) Calculate X_{S_i} using the scanned object's geometrical properties and r_i or l_i, where $i = 1, 2, \cdots, n$.
   (b) Calculate the AUV positions x_i using X_{S_i} and ψ_S, where $i = 1, 2, \cdots, n$.

2.2.2. *Sway motion.* Although the hexagonal scanned object for surge motion is also applicable to the sway scenario, the simplest scanned object for the sway motion is a rectangular board, as shown in Figure 4. The procedure to calculate the AUV positions during sway motion is as follows:

1. For point A (or B) on each of the n laser images, convert its horizontal pixel coordinate to the horizontal coordinate ξ_i on the laser scanning plane, where $i = 1, 2, \cdots, n$.
2. Use ξ_1 as the initial point to calculate the AUV positions y_i via Equation (2) as below:

$$y_i = \xi_i - \xi_1 \tag{2}$$

where $i = 1, 2, \cdots, n$.

https://doi.org/10.1017/S0373463318000139 Published online by Cambridge University Press

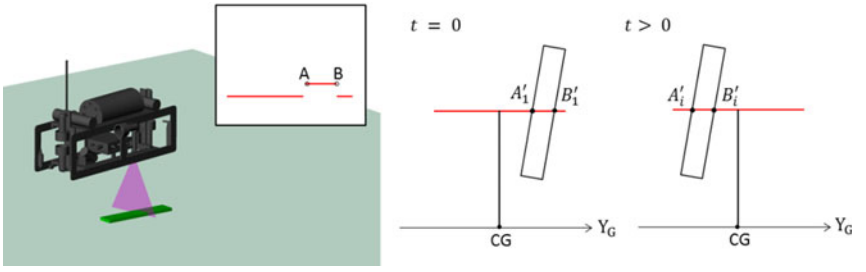

Figure 4. Laser image-based AUV position calculation for sway motion.

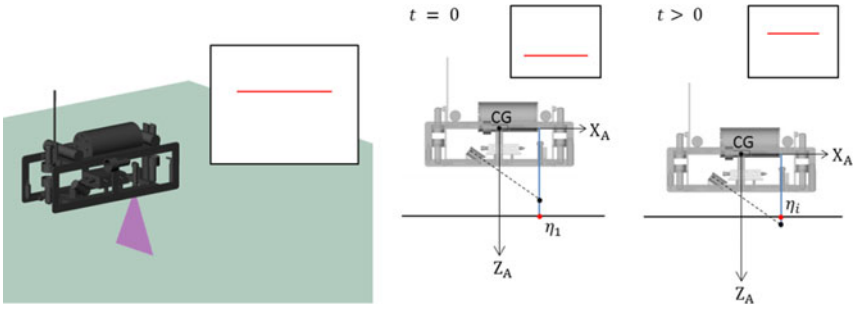

Figure 5. Laser image-based AUV position calculation for heave motion.

2.2.3. *Heave motion.* A laser line moves vertically in the images as the AUV undergoes a heave motion. As shown in Figure 5, the laser line moves up as the AUV goes down. The procedure to calculate the AUV positions in heave motion is as follows:

1. For each of the n laser images, obtain the laser line's vertical coordinate η_i on the laser scanning plane, where $i = 1, 2, \cdots, n$.
2. Use η_1 as the initial point to calculate the AUV positions z_i via Equation (3) as below:

$$z_i = \eta_i - \eta_1 \tag{3}$$

where $i = 1, 2, \cdots, n$.

2.2.4. *Roll motion.* A laser line rotates in the images as the AUV undergoes roll motion. As shown in Figure 6, the laser line rotates counterclockwise as the AUV rolls clockwise. The procedure to calculate the AUV Euler angles in roll motion is as follows:

1. For points A and B on each of the n laser images, convert their planar pixel coordinates to the planar coordinates (ξ_i, η_i) on the laser scanning plane, where $i = 1, 2, \cdots, n$.
2. Calculate the AUV Euler angles ϕ_i using Equation (4) as below:

$$\tan \phi_i = \frac{\eta_{i_B} - \eta_{i_A}}{\xi_{i_A} - \xi_{i_B}} \tag{4}$$

where $i = 1, 2, \cdots, n$.

https://doi.org/10.1017/S0373463318000139 Published online by Cambridge University Press

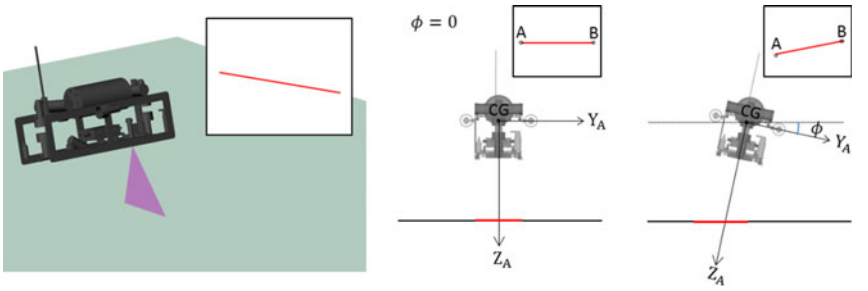

Figure 6. Laser image-based AUV attitude calculation for roll motion.

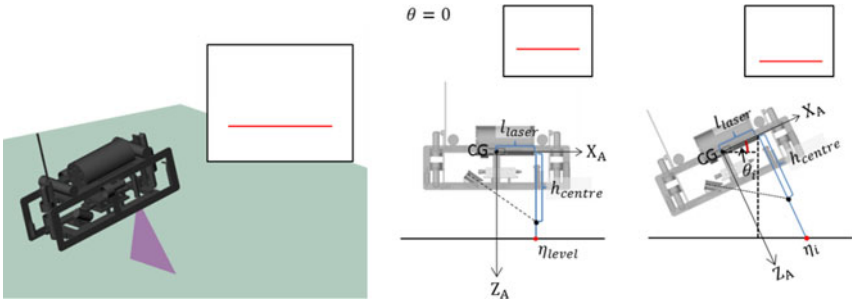

Figure 7. Laser image-based AUV attitude calculation for pitch motion.

2.2.5. *Pitch motion.* A laser line moves vertically in the images as the AUV undergoes a pitching motion. As shown in Figure 7, the laser line moves down as the AUV pitches up. The procedure to calculate the AUV Euler angles in the pitch motion is as follows:

1. For each of the n laser images, obtain the laser line's vertical coordinate η_i on the laser scanning plane, where $i = 1, 2, \cdots, n$.
2. Calculate the AUV Euler angles θ_i using Equation (5) as below, where η_{level} is the laser line's position at $\theta = 0$:

$$(h_{centre} - \eta_i)\cos\theta_i = l_{laser}\sin\theta_i + h_{centre} - \eta_{level} \tag{5}$$

2.2.6. *Yaw motion.* The scanned object for yaw motion is the same as for surge motion, as shown in Figure 8. The procedure to calculate the AUV Euler angles during yaw motion is as follows:

(a) – (c) The same as those in step 1 for surge motion.

(d) Use ψ_{S_1} as the initial angle to calculate the AUV Euler angles ψ_i via Equation (6) as below:

$$\psi_i = \psi_{S_i} - \psi_{S_1} \tag{6}$$

where $i = 1, 2, \cdots, n$.

2.3. *Evolutionary search for hydrodynamic parameters.* Genetic Algorithms (GAs) always operate on a whole population of candidates rather than a single candidate for solution searching. This characteristic improves the chances of a GA reaching the global

https://doi.org/10.1017/S0373463318000139 Published online by Cambridge University Press

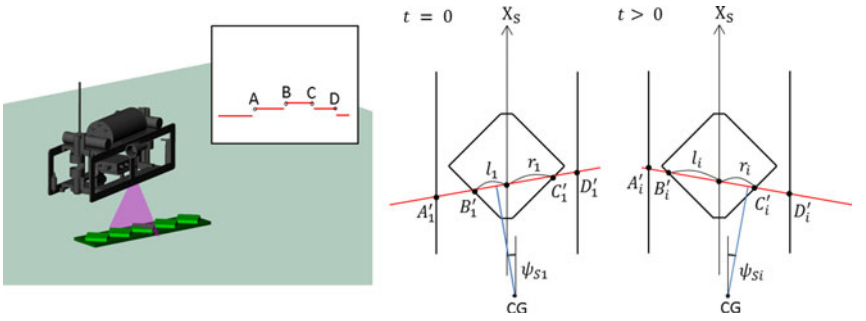

Figure 8. Laser image-based AUV attitude calculation for yaw motion.

optimum and also helps GAs avoid being trapped in a local optimum. This characteristic also indicates the inherent parallelism of GAs, which facilitates the distributed implementation of GAs for computational efficiency enhancement (Sivanandam and Deepa, 2007). A basic GA was implemented in this research to validate the feasibility of the proposed method, LSHPI. Nevertheless, any evolutionary optimisation algorithm can be used in LSHPI. Here, the GA has six objective functions, each of which corresponds to a 1D motion. Thus, for a specific 1D motion, the GA takes the positions or Euler angles obtained through laser images as the input and returns a set of hydrodynamic parameters that minimise the motion's objective function value. As an example, the objective function for surge motion is illustrated below.

The system of equations relating $X_A Y_A Z_A$ to $X_G Y_G Z_G$ for surge motion is as follows:

$$\begin{cases} \dot{u} = \left[\left(X_u + X_{u|u|}\,|u|\right) u + X\right] / \left(m - X_{\dot{u}}\right) \\ \dot{x} = u \end{cases} \tag{7}$$

The position dataset obtained from the laser images is defined as:

$$\mathrm{x}_{img} = \left\{ x^i_{img} \,|i = 1 \sim n \right\} \tag{8}$$

where x^i_{img} is the i-th position value.

The position dataset obtained from Equation (7) with a set of hydrodynamic parameters, $\{X_{\dot{u}}, X_u, X_{u|u|}\}$, is defined as:

$$\mathrm{x}_{eof} = \left\{ x^i_{eof} \,|i = 1 \sim n \right\} \tag{9}$$

where x^i_{eof} is the i-th position value.

Therefore, the objective function for the surge motion is defined as:

$$f\left(X_{\dot{u}}, X_u, X_{u|u|}\right) = \sum_{i=1}^{n} \left| x^i_{eof} - x^i_{img} \right| \tag{10}$$

3. FEASIBILITY VALIDATION OF LSHPI THROUGH OPENGL LASER IMAGES.

In this research, laser images, seen from an on board camera's perspective and created using Open Graphics Library (OpenGL) (Wright et al., 2010), are used to validate the feasibility of the proposed LSHPI. To this end, the subsequent subsections will present the

https://doi.org/10.1017/S0373463318000139 Published online by Cambridge University Press

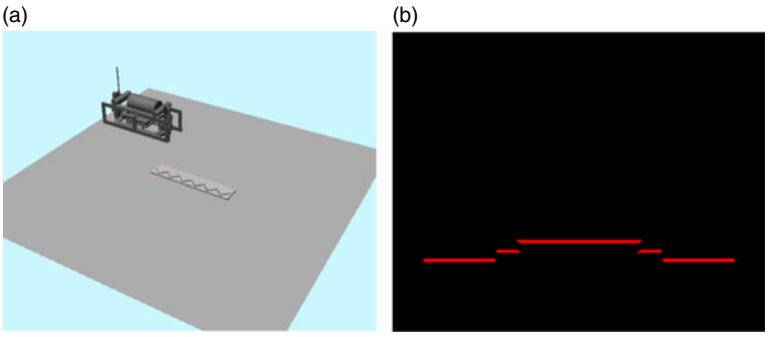

Figure 9. (a) An elevation view of the AUV; (b) a laser image seen from the AUV camera.

following topics: 3.1. Laser images created by OpenGL; 3.2. Coordinate transformation from the image plane to the laser scanning plane; 3.3. Comparison between the OpenGL and experimental measurement results; 3.4. Accuracy for the laser image-based AUV position and attitude calculations; 3.5. Effect of motion disturbances on the laser image-based AUV position and attitude calculations and finally 3.6. Identification of surge-related hydrodynamic parameters by the proposed LSHPI.

3.1. *Laser images created by OpenGL.* OpenGL models a spotlight source as restricted to producing a cone of light in a particular direction. In this research, a line-laser is modelled based on the OpenGL spotlight model, such that the line-laser produces a beam of light with a fan angle of 40° and line thickness of 6 mm. In addition, only the diffuse effect of the laser light is considered in this research. For instance, in Figure 9, the left sub-figure shows an elevation view of the AUV, which performs surge motion and projects a laser light stripe on a hexagon object; the right sub-figure shows a laser image that is seen from the AUV on board camera and consists of several laser line segments, and the discontinuity points on the laser line represent the locations where the object height changes.

3.2. *Transformation from image plane coordinates to laser scanning plane coordinates.* Figure 10 shows the viewing volume of the camera for creating laser images by OpenGL. A laser image is the current view of the laser scanning plane seen from the camera. In this research, a laser image is specified to have 720 × 576 pixels; in the vertical direction, a laser line has a width of several pixels, and the central pixel is chosen to be the laser line's position.

The transformation from the image plane coordinates to the laser scanning plane coordinates is illustrated as follows:

1. Transform the image plane coordinates $(\tilde{i}, \tilde{j})$ to the near clipping plane coordinates $(\tilde{x}, \tilde{y})$ using ω and h, where ω is the angle of the camera's field of view on the $\eta - \zeta$ plane and h is the distance from the viewpoint to the near clipping plane.
2. Transform the near clipping plane coordinates $(\tilde{x}, \tilde{y})$ to the laser scanning plane coordinates (ξ, η) through Equations (11) and (12):

$$\eta = \eta_c + \frac{h\cos\alpha - \tilde{y}\sin\alpha}{h\sin\alpha + \tilde{y}\cos\alpha}\zeta_c \tag{11}$$

https://doi.org/10.1017/S0373463318000139 Published online by Cambridge University Press

$$\xi = \frac{\sqrt{\zeta_c^2 + (\eta_c - \eta)^2}}{\sqrt{(h\sin\alpha + \tilde{y}\cos\alpha)^2 + (h\cos\alpha - \tilde{y}\sin\alpha)^2}}\tilde{x} \tag{12}$$

where (η_c, ζ_c) is the camera's coordinates on the $\eta - \zeta$ plane.

Table 2 lists the lengths and angle denoting the geometrical relations between the CG, video camera and the AUV laser module previously shown in Figure 2. Moreover, Figure 11 shows the dimensions of the scanned object that consists of six hexagonal components on top of a rectangular board and will be used for surge and yaw motions.

3.3. *Comparison between OpenGL and experimental measurement results.* With the proposed LSHPI, the AUV positions and Euler angles are all obtained through laser images. In this research, the feasibility of LSHPI will be validated using the laser images created by OpenGL. Therefore, it is important to compare the measurement errors between the OpenGL measurement results and experimental measurement results. If the OpenGL measurement errors are larger than but close to the real-world measurement errors, the OpenGL measurement results can then be considered to properly include errors from the uncertainty and nonlinearity factors, such as the lens distortion, the roughness of the scanned object, the nonlinearities of the laser beam, etc, as experienced in real-world experiments.

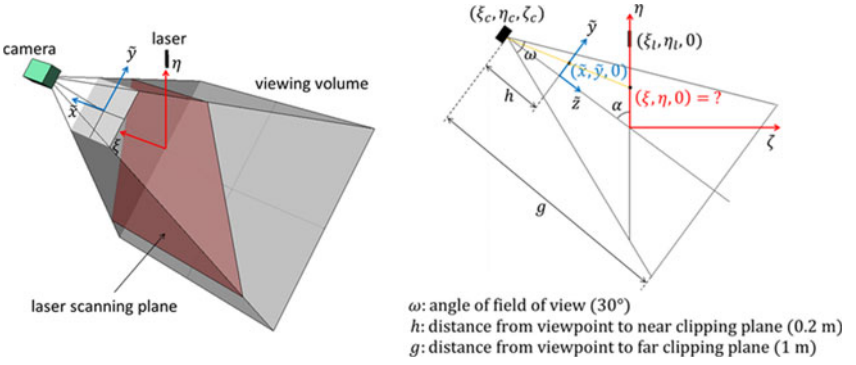

Figure 10. Viewing volume of the camera for creating laser images.

Table 2. Lengths and angle used in Figure 2.

l_{laser}	0·27 m
l_{camera}	0·19 m
h_{camera}	0·22 m
h_{centre}	0·68 m
α	45°

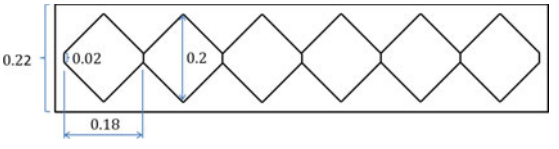

Figure 11. Dimensions (in metres) of the scanned object for the surge and yaw motions.

https://doi.org/10.1017/S0373463318000139 Published online by Cambridge University Press

Table 3. Accuracy for laser image-based postion and atttiude calculations in decoupled AUV motions.

		Moving conditions				
		Range	Increment	Distance from floor to AUV's CG	ψ_S	Error range (mm, deg)
Surge	x	$0 \sim 200$ mm	1 mm	830 mm	0°	$-0{\cdot}8 \leq \Delta x_{error} \leq 0{\cdot}7$
Sway	y	$0 \sim 280$ mm	1 mm	830 mm	0°	$-0{\cdot}2 \leq \Delta y_{error} \leq 0{\cdot}6$
Heave	z	$0 \sim 420$ mm	1 mm	930 mm (initial distance)		$-0{\cdot}6 \leq \Delta z_{error} \leq 0{\cdot}7$
Roll	ϕ	$-20 \sim 20°$	0·1°	680 mm		$-0{\cdot}2 \leq \Delta \phi_{error} \leq 0{\cdot}2$
Pitch	θ	$-20 \sim 20°$	0·1°	680 mm		$-0{\cdot}2 \leq \Delta \theta_{error} \leq 0{\cdot}7$
Yaw	ψ	$0 \sim 34°$	0·1°	830 mm	−17°	$-0{\cdot}6 \leq \Delta \psi_{error} \leq 0{\cdot}8$

In this research, a test object, with the same shape and dimensions as those in Wang and Cheng (2007), is created using OpenGL. Then, the dimension measurements are performed through a laser image seen from the on board camera of a stationary AUV. According to the results, the absolute error for the OpenGL-measured dimensions ranges from 0·08 mm to 1·14 mm, whereas the absolute error for the dimensions obtained through real-world experiments in Wang and Cheng (2007) ranges from 0·07 mm to 0·66 mm. The OpenGL absolute error range is larger than the experimental absolute error range, but the two error ranges have the same order of magnitude. Therefore, the OpenGL measurement results can be considered to adequately include errors contributed by the uncertainty and nonlinearity factors associated with the camera, the scanned object and the laser beam, as encountered in the real-world experiments.

3.4. *Accuracy for laser image-based AUV position and attitude calculations.* In order to investigate the accuracy of the AUV positions and Euler angles obtained by the laser image-based methods illustrated in Section 2, OpenGL animations were implemented and executed. In each OpenGL animation, an AUV performed a 1D motion under the conditions listed in Table 3.

For each 1D motion, the calculated positions or Euler angles were compared with actual results to obtain an error range, as shown in Table 3. According to the results, for surge, sway and heave motions, the maximum absolute errors were all less than 1 mm; for roll, pitch and yaw motions, the maximum absolute errors were all less than 1°.

3.5. *Influence of motion disturbances on laser image-based AUV position and attitude calculations.* Conducting a specific 1D AUV motion experiment in a water tank usually involves other motion disturbances. Such disturbances will change the laser line locations displayed in laser images, affecting the accuracy of the AUV positions or Euler angles acquired by the proposed laser image-based methods. Therefore, OpenGL animations are implemented and executed, with the moving conditions listed in Table 3 and disturbances listed in Table 4 (or Table 5). Additionally, the term "no effect" in Table 4 and Table 5 means that a specific motion disturbance has no influence on the accuracy for the positions or Euler angles obtained in a particular 1D motion.

For surge motion, the sway disturbance affects the accuracy of calculated AUV positions if a yaw disturbance exists. Likewise, heave disturbance affects the accuracy of calculated AUV positions if a pitch disturbance exists. Moreover, roll, pitch and yaw disturbances all influence the accuracy of calculated AUV positions. Compared with other errors, the maximum error induced by the pitch disturbance is significant.

For sway motion, the surge disturbance affects the accuracy of calculated AUV positions if the scanned object's centreline is not perpendicular to the sway direction. Compared with

https://doi.org/10.1017/S0373463318000139 Published online by Cambridge University Press

Table 4. Influence of motion disturbances on the accuracy for calculated AUV positions.

		Maximum absolute error		
	Disturbance	Surge Δx_{error}	Sway Δy_{error}	Heave Δz_{error}
Surge	$-10 \le \Delta x_d \le 10$ (mm)		0·9 mm (if $\psi_S = 5^\circ$)	no effect
Sway	$-10 \le \Delta y_d \le 10$ (mm)	2·9 mm (if $\Delta\psi_d = 5$)		no effect
Heave	$-10 \le \Delta z_d \le 10$ (mm)	0·5 mm (if $\Delta\theta_d = 1^\circ$)	no effect	
Roll	$-1 \le \Delta\phi_d \le 1$ (deg)	1·5 mm	15 mm	1·1 mm
Pitch	$-1 \le \Delta\theta_d \le 1$ (deg)	15 mm	1·5 mm (if $\psi_S = 5^\circ$)	6 mm
Yaw	$0 \le \Delta\psi_d \le 5$ (deg)	2 mm (if $Y_S = 0$, $\psi_S = 0$)	23 mm	no effect

Table 5. Influence of motion disturbances on the accuracy for calculated AUV Euler angles.

		Maximum absolute error		
	Disturbance	Roll $\Delta\phi_{error}$	Pitch $\Delta\theta_{error}$	Yaw $\Delta\psi_{error}$
Surge	$-10 \le \Delta x_d \le 10$ (mm)	no effect	no effect	no effect
Sway	$-10 \le \Delta y_d \le 10$ (mm)	no effect	no effect	no effect
Heave	$-10 \le \Delta z_d \le 10$ (mm)	no effect	shown in Figure 12	no effect
Roll	$-1 \le \Delta\phi_d \le 1$ (deg)		0·5°	1·1°
Pitch	$-1 \le \Delta\theta_d \le 1$ (deg)	no effect		no effect
Yaw	$0 \le \Delta\psi_d \le 5$ (deg)	no effect	no effect	

other errors, the maximum errors, induced by roll and yaw disturbances, respectively, are both significant.

Figure 12 shows the calculated pitch angles when the AUV pitches up with two different heave disturbances; the calculated AUV pitch angles with a downward heave disturbance are displayed in blue dots, whereas the calculated AUV pitch angles with an upward heave disturbance are displayed in green dots. The absolute errors between the actual and calculated pitch angles at $\theta = 20^\circ$ and $\theta = -15^\circ$ are also shown in Figure 12. Such an absolute error increases significantly when the pitch angle θ becomes negative. This is because, without any motion disturbances, the rate of change of laser line position (η) on the laser scanning plane becomes small when the pitch angle θ turns negative, as shown in Figure 13 As a result, if a heave disturbance exists, when the pitch angle θ becomes negative, the effect of the heave disturbance on the change of laser line position also becomes significant.

3.6. *Hydrodynamic parameter identification for surge motion by LSHPI.* This section considers surge motions under three conditions: (1) no motion disturbances exist; (2) a pitch disturbance exists; (3) pitch and yaw disturbances both exist. The influence of the pitch and yaw disturbances on the accuracy of the surge-related hydrodynamic parameters obtained by the LSHPI will be investigated. Table 6 shows the physical properties and the surge-related hydrodynamic parameters of an AUV. The parameters, including $X_{\dot{u}} = -250$, $X_u = -20$ and $X_{u|u|} = -200$, are defined as the actual hydrodynamic parameters in this work.

3.6.1. *AUV position datasets for OpenGL animations.* In this research, position datasets used to move the AUV in OpenGL animations are created by solving the equation of surge motion, with parameters listed in Table 6 and a resultant force X from thrusters,

https://doi.org/10.1017/S0373463318000139 Published online by Cambridge University Press

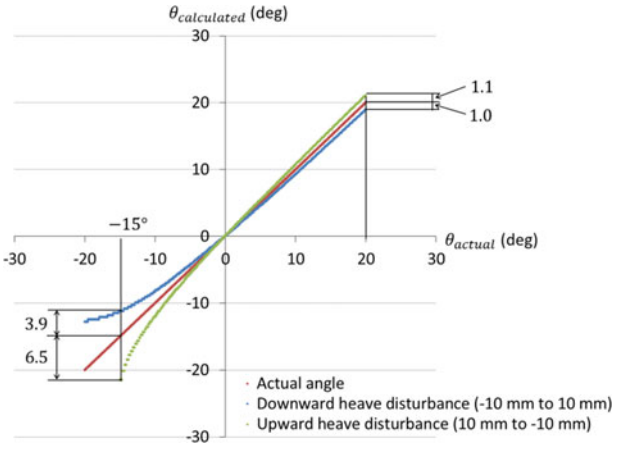

Figure 12. Relations between actual and calculated pitch angles with different heave disturbances.

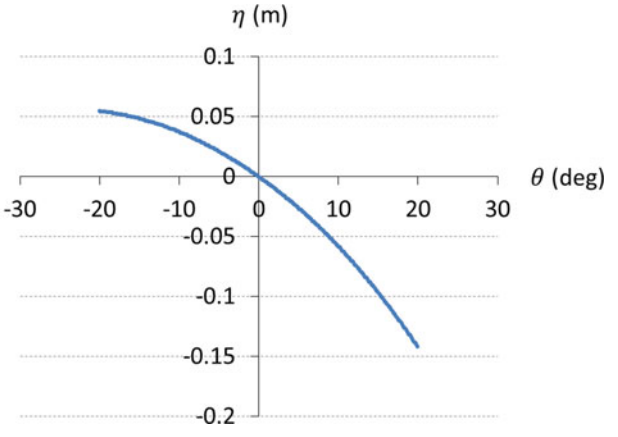

Figure 13. Relations between pitch angle and laser line position on the laser scanning plane without disturbances.

Table 6. Physical properties and surge-related hydrodynamic parameters of an AUV.

m	29·777 (kg)
I_x	0·730 (kg · m^2)
I_y	2·352 (kg · m^2)
I_z	2·144 (kg · m^2)
r_{B_Z}	−0·028 (m)
$X_{\dot{u}}$	−250 (kg)
X_u	−20 (kg/s)
$X_{u\|u\|}$	−200 (kg/m)

using the fourth-order Runge-Kutta method. Such position datasets are defined as actual position datasets in this work. Figure 14 shows two actual position datasets obtained for $X = 4$ N and $X = 8$ N, respectively. For surge animations with pitch disturbances, a total of two position datasets are created by adding the pitch disturbance data, shown in

https://doi.org/10.1017/S0373463318000139 Published online by Cambridge University Press

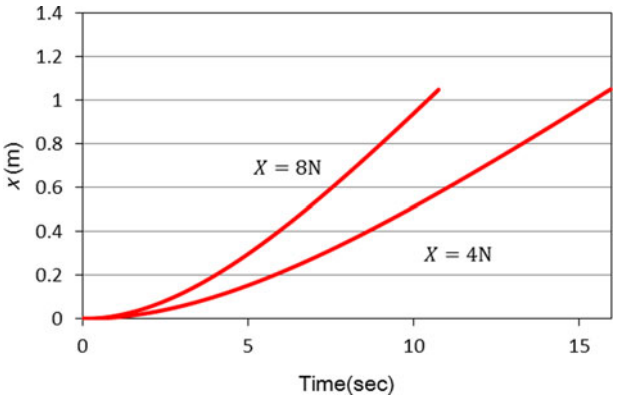

Figure 14. Actual position datasets for a 1-metre surge motion at $X = 4$ N and $X = 8$ N.

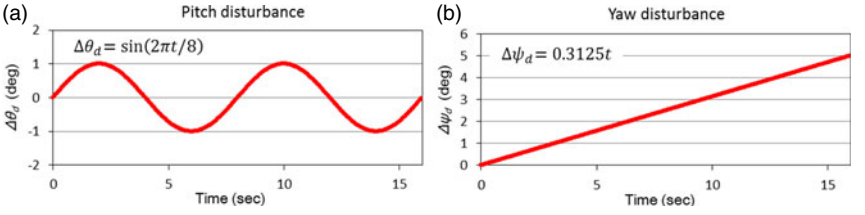

Figure 15. Artificial pitch and yaw disturbances for surge motion at $X = 4$ N.

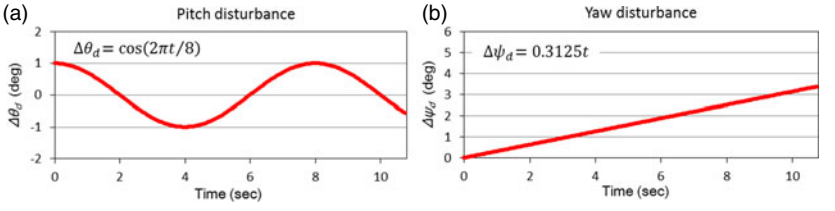

Figure 16. Artificial pitch and yaw disturbances for surge motion at $X = 8$ N.

Figure 15(a) and Figure 16(a), to the actual position data for $X = 4$ N and $X = 8$ N, respectively. Likewise, for surge animations with both pitch and yaw disturbances, a total of two position datasets are created by adding both pitch and yaw disturbance data, shown in Figure 15 and Figure 16, to the actual position data for $X = 4$ N and $X = 8$ N, respectively.

3.6.2. *AUV positions obtained from laser images.* As illustrated in the previous subsection, a total of six OpenGL animations were created for AUV surge motions under three disturbance conditions and two thrust conditions. The laser images taken in each animation are used to obtain the AUV positions for the corresponding surge motion. Additionally, in each animation, the angle ψ_S between the AUV moving path and the scanned object's centreline is set as -4°.

At each time step, the angle ψ_{S_i} between the AUV moving path and the scanned object's centreline can be obtained from each laser image. For example, Figure 17 shows the obtained angles $\psi_{S_i}(i = 1, 2, \ldots)$ at $X = 4$ N under two different conditions: (1) the AUV moves without disturbances; (2) the AUV moves with both pitch and yaw disturbances. The results illustrate that it is feasible to use the proposed hexagonal scanned object to obtain the

https://doi.org/10.1017/S0373463318000139 Published online by Cambridge University Press

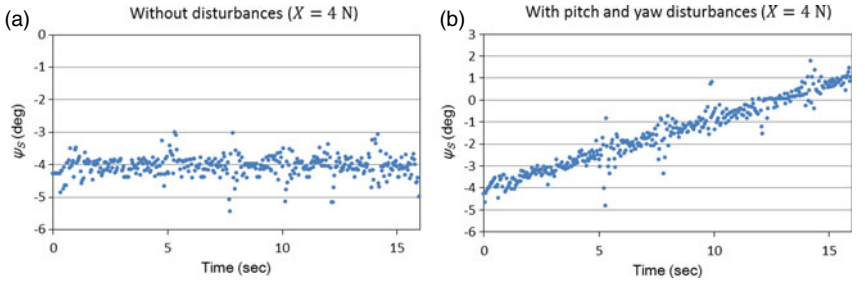

Figure 17. $\psi_{S_i}(i = 1, 2, \ldots)$ obtained from laser images.

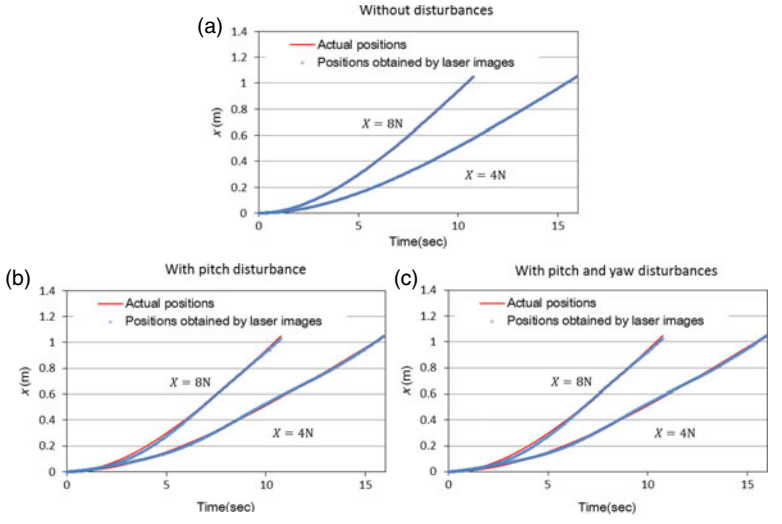

Figure 18. AUV actual positions and positions obtained from laser line images.

Table 7. ψ_S and maximum absolute position error for each of the six surge motions.

	X = 4 N		X = 8 N	
	ψ_S	Maximum absolute position error	ψ_S	Maximum absolute position error
Surge only	−4·05°	1.0 mm	−4·08°	1.0 mm
Surge with pitch disturbance	−4·07°	14·6 mm	−4·05°	29·7 mm
Surge with pitch and yaw disturbances	−1·53°	15·4 mm	−2·36°	27·9 mm

angles ψ_{S_i} $(i = 1, 2, \ldots)$ and that the deviation from the correct angle value becomes larger when the AUV is passing the common narrow side of two connected hexagon components.

Figure 18 shows the actual positions and the positions obtained from laser images for the six surge motions with different combinations of thrust and motion disturbance. Table 7 shows the obtained angle ψ_S and the maximum absolute position error in each of the six surge motions. As illustrated earlier in Section 2, the angle ψ_S is the average value of $\psi_{S_i}(i = 1, 2, \ldots)$ and is used to calculate the AUV positions in surge motion.

https://doi.org/10.1017/S0373463318000139 Published online by Cambridge University Press

Table 8. Settings of the GA's parameters.

Size of the candidate population	500
Crossover probability	0·8
Mutation probability	0·15
No. of iterations	2,000

Table 9. Search range of each hydrodynamic parameter in the GA.

Surge motion	$X_{\dot{u}}$	[−500 0]
	X_u	[−100 0]
	$X_{u\|u\|}$	[−500 0]

Table 10. Hydrodynamic parameters identified for three disturbance conditions.

	$X_{\dot{u}}$	X_u	$X_{u\|u\|}$
Actual parameters	−250	−20	−200
Surge only	−250·061	−20·0488	−199·512
Surge with pitch disturbance	−258·120	−18·8034	−208·059
Surge with pitch and yaw disturbances	−256·532	−18·9499	−212·454

Table 11. Max. absolute errors between actual and identified-parameter-based positions for 5-m surge motions.

	Maximum absolute position error and percentage error		
	X = 4 N	X = 8 N	X = 16 N
Surge only	0·4 mm	1·1 mm	2·1 mm
	0·01 %	0·02 %	0·04 %
Surge with pitch disturbance	17·5 mm	17·1 mm	42·7 mm
	0·35 %	0·34%	0·85 %
Surge with pitch and yaw disturbances	21·7 mm	55·5 mm	80·4 mm
	0·42 %	1·11 %	1·61 %

3.6.3. *GA search for hydrodynamic parameters.* The surge-related hydrodynamic parameters are determined through a GA search strategy. The GA takes X = 4 N and X = 8 N position datasets as two inputs and uses the sum of two normalised objective function values as the quality index for each candidate solution, that is, each hydrodynamic parameter set containing $X_{\dot{u}}$, X_u, and $X_{u|u|}$. As previously illustrated in Section 2, the smaller the objective function value, the better the solution quality.

Table 8 shows the settings of the GA's parameters. Table 9 shows the search range of each hydrodynamic parameter in the GA. Taking position datasets regarding two thrust conditions as inputs, the GA aims to find a set of hydrodynamic parameters for each of the three disturbance conditions: (1) surge motion without disturbances; (2) surge motion with pitch disturbance and (3) surge motion with both pitch and yaw disturbances. For each of the above conditions, the GA is executed ten times to generate ten optimal hydrodynamic parameter sets among which the best set is selected as the identification result.

Table 10 shows the hydrodynamic parameters identified for the three disturbance conditions. When no disturbances exist, the obtained hydrodynamic parameters are very close

https://doi.org/10.1017/S0373463318000139 Published online by Cambridge University Press

to the actual parameters. Meanwhile, when a pitch disturbance exists or pitch and yaw disturbances both exist, the obtained hydrodynamic parameters show some differences from the actual parameters.

In order to evaluate the effectiveness of the identified hydrodynamic parameters, the positions for a long surge motion, that is, a 5 metre surge motion, are calculated using the three sets of identified hydrodynamic parameters, shown in Table 10, under three different thrusts, $X = 4$ N, $X = 8$ N and $X = 16$N.

The maximum absolute errors between the actual positions and the positions calculated through the identified hydrodynamic parameters are shown in Table 11. The largest absolute error, 80·4 mm, comes from the positions calculated by the hydrodynamic parameters obtained when pitch and yaw disturbances both exist. However, the percentage error for the above absolute error is calculated as 1·61%, which can be considered insignificant. Therefore, the above results indicate that the proposed LSHPI can be used to identify AUV hydrodynamic parameters with sufficient accuracy under moderate motion disturbances.

4. CONCLUSIONS. This paper presents a new method, Laser Line Scanning for Hydrodynamic Parameter Identification (LSHPI), which integrates laser line scanning, decoupled dynamics and evolutionary optimisation to identify AUV hydrodynamic parameters. The AUV dynamic model, the laser image-based AUV position and attitude calculations for six 1D motions and the GA adopted to search for hydrodynamic parameters have all been illustrated in the paper.

In this research, laser images, seen from an on board camera's perspective and created using OpenGL, were used to validate the feasibility of the proposed LSHPI. Firstly, through the comparison between the OpenGL measurement results and the experimental measurement results, which were obtained from laser images captured by a stationary camera, the OpenGL measurement results were considered to adequately include errors from the uncertainty and nonlinearity factors associated with the camera, the scanned object, and the laser beam, as encountered in the real-world experiments. Secondly, the accuracy for the AUV positions and Euler angles obtained by the laser image-based methods were investigated. In addition, for each decoupled 1D motion, the influence of other motion disturbances on the accuracy for the AUV positions or Euler angles obtained was also evaluated. Finally, the accuracy for the surge-related hydrodynamic parameters obtained by the LSHPI was investigated under three different conditions: (1) no motion disturbances exist; (2) pitch disturbance exists and (3) pitch and yaw disturbances both exist.

According to the hydrodynamic parameters obtained under different motion disturbance conditions, it is concluded that the proposed LSHPI can be used to identify AUV hydrodynamic parameters with sufficient accuracy under moderate motion disturbances. As a result, this research has validated the feasibility of applying laser line scanning to the identification of AUV hydrodynamic parameters.

FINANCIAL SUPPORT

This research is supported by the Ministry of Science and Technology of Taiwan, under grants MOST 106-2221-E-110-042, MOST 105-2221-E-110-060, MOST 104-2221-E-110-062, MOST 107-3113-M-110-001, MOST 106-3113-M-110-001, and MOST 105-3113-M-110-001.

REFERENCES

Avila, J.J., Nishimoto, K., Sampaio, C.M. and Adamowski, J.C. (2012). Experimental investigation of the hydrodynamic coefficients of a remotely operated vehicle using a planar motion mechanism. *Journal of Offshore Mechanics and Arctic Engineering*, **134**, 0216011–0216016.

Avila, J.P., Donha, D.C. and Adamowski, J.C. (2013). Experimental model identification of open-frame underwater vehicles. *Ocean Engineering*, **60**, 81–94.

Caccia, M., Indiveri, G. and Veruggio, G. (2000). Modeling and identification of open-frame variable configuration unmanned underwater vehicles. *IEEE Journal of Oceanic Engineering*, **25**, 227–240.

Caccia, M. and Veruggio, G. (2000). Guidance and control of a reconfigurable unmanned underwater vehicle. *Control Engineering Practice*, **8**, 21–37.

Chen, H.-H. (2008). Vision-based tracking with projective mapping for parameter identification of remotely operated vehicles. *Ocean Engineering*, **35**, 983–994.

Farrell, J. and Clauberg, B. (1993). Issues in the implementation of an indirect adaptive control system. *IEEE Journal of Oceanic Engineering*, **18**, 311–318.

Fossen, T.I. (1994). *Guidance and control of ocean vehicles*. Wiley New York.

Gracias, N.R., Van Der Zwaan, S., Bernardino, A. and Santos-Victor, J. (2003). Mosaic-based navigation for autonomous underwater vehicles. *IEEE Journal of Oceanic Engineering*, **28**, 609–624.

Martin, S.C. and Whitcomb, L.L. (2014). Experimental Identification of Six-Degree-of-Freedom Coupled Dynamic Plant Models for Underwater Robot Vehicles. *IEEE Journal of Oceanic Engineering*, **39**, 662–671.

Nakamura, M., Asakawa, K., Hyakudome, T., Kishima, S., Matsuoka, H. and Minami, T. (2013). Hydrodynamic Coefficients and Motion Simulations of Underwater Glider for Virtual Mooring. *IEEE Journal of Oceanic Engineering*, **38**, 581–597.

Negahdaripour, S. and Xu, X. (2002). Mosaic-based positioning and improved motion-estimation methods for automatic navigation of submersible vehicles. *IEEE Journal of Oceanic Engineering*, **27**, 79–99.

Nomoto, M. and Hattori, M. (1986). A deep ROV Dolphin 3K: design and performance analysis. *IEEE Journal of Oceanic Engineering*, **11**, 373–391.

Ridao, P., Tiano, A., El-Fakdi, A., Carreras, M. and Zirilli, A. (2004). On the identification of non-linear models of unmanned underwater vehicles. *Control Engineering Practice*, **12**, 1483–1499.

Sivanandam, S. and Deepa, S. (2007). *Introduction to genetic algorithms*. Springer Science & Business Media.

Smallwood, D.A. and Whitcomb, L.L. (2003). Adaptive identification of dynamically positioned underwater robotic vehicles. *IEEE Transactions on Control Systems Technology*, **11**, 505–515.

Valeriano-Medina, Y., Martínez, A., Hernández, L., Sahli, H., Rodríguez, Y. and Cañizares, J. (2013). Dynamic model for an autonomous underwater vehicle based on experimental data. *Mathematical and Computer Modelling of Dynamical Systems*, **19**, 175–200.

Wang, C.-C. and Cheng, M.-S. (2007). Nonmetric camera calibration for underwater laser scanning system. *IEEE Journal of Oceanic Engineering*, **32**, 383–399.

Wright, R.S., Haemel, N., Sellers, G. and Lipchak, B. (2010). *OpenGL SuperBible: Comprehensive Tutorial and Reference*. Addison-Wesley Professional.